Quantification of in-plane stress development during drying of tape-cast ceramic layers by cantilever deflection method

P.-M. Geffroy, H. Schubert, J. Günster, A. Zocca

Quantification of in-plane stress development during drying of tape-cast ceramic layers by cantilever deflection method

P.-M. Geffroy[1,2*], H. Schubert[1], J. Günster[1,3] and A. Zocca[1]

[1] *Bundesanstalt für Materialforschung und -prüfung (BAM), 5.4 Division Advanced Multi-materials Processing, Unter den Eichen 87, 12205, Berlin, Germany*

[2] *CNRS, Institut de Recherche sur les Céramiques (IRCER), UMR 7315, Centre Européen de la Céramique, 12 rue Atlantis, 87068 LIMOGES Cedex, France*

[3]*Institute of Non-Metallic Materials, Clausthal University of Technology, 38678 Clausthal-Zellerfeld, Germany*

*Corresponding author. Dr. Pierre-Marie Geffroy, Tel: +33(5)40002753; fax: +33(5)40002761;

e-mail address: pierre-marie.geffroy@unilim.fr

Abstract

The control of stress development in cast ceramics during drying is usually one of critical steps in ceramic processes, which is important also for additive manufacturing technologies using a suspension as feedstock. This work introduces a method based on the cantilever deflection method, to quantify simultaneous the kinetics of solvent evaporation, the shrinkage and the intensity of in-plane stresses developed during drying. Particular attention is given here to the experimental limits of the method and the optimization of experimental conditions to measure suitably the intensity of in-planar stress in the coating. The optimized method is applied to four alumina slurries for the water-based additive manufacturing technology LSD-print. Four stages of drying are identified and discussed in relation with the granulometry and morphology of the alumina ceramic particles.

Key words: In-plane stresses, drying, kinetics of drying, cantilever deflection method

1. Introduction

The drying of ceramic parts is a common critical step in ceramic processes, because the development of capillary stresses between particles during the last step of drying can lead to micro-cracks in green part, which will develop into defects in the final sintered part. The formation of these defects often leads to the degradation of properties or performances of ceramic parts. For this reason, the understanding of crack formation mechanisms in green ceramic part during the drying is an important field in material sciences, with a huge economic impact in many industrial sectors. In the conventional theory of drying [1], the origin of cracks is linked to the development of capillary stresses in the particle network, which results from the formation of a meniscus of solvent between ceramic particles during the evaporation step. The capillary stress, P can be expressed as following according to the Young-Laplace equation:

$$P = \frac{2\gamma\cos\theta}{r_p} \qquad (1)$$

where r_p is the radius of pores, γ is surface tension, and θ is wetting angle of solvent with the solid particles.

A subset of the general theory of drying of ceramic bodies is constituted by the drying of ceramic layers, which is of high relevance in the fabrication of ceramic coatings and for the tape casting process. A newer field of application also concerns the additive manufacturing of ceramics by slurry-based binder jetting technologies, in which layers of a water-based ceramic slurry are deposited, dried and selectively printed by ink jetting. The method used to deposit a layer can be by spraying, such as originally developed by Cima et al. [2] or by doctor blade, such as in the layerwise slurry deposition (LSD-print) process [3,4].

During drying of thin ceramic layers, the in-plane shrinkage is constrained by the substrate, which results in the development of a biaxial stress. In a brittle material this biaxial stress can cause the fracture of the layer by nucleation and growth of one or several cracks. Hu et al. [5] developed a model starting from fracture mechanics considerations, following the concept that a crack will not grow until the energy needed to extend the crack is less than the energy released when relieving the elastic strain in the layer. From this model, it follows that there is a critical thickness (h_{max}) above which a layer will crack during drying:

$$h_{max} = \left(\frac{K_c}{1.4\,\sigma}\right)^2 \quad (2)$$

Where K_c is the fracture resistance of the layer and σ is the biaxial stress at fracture. More complex models, e.g. by Singh and Tirumkudulu [6], have been introduced to relate h_{max} to the microscopic properties of the granular system, including the capillary pressure, the elastic properties of the particles and their radius and packing. Equation (2) indicates that there are only three possible main strategies to eliminate cracking during drying of ceramic layers: (i) reduce the layer thickness, (ii) increase the layer strength, e.g. by the addition of binders and (iii) reduce or relax the biaxial stress (which is proportional to the capillary pressure), e.g. by increasing the particle size, by adding surfactants [7] or by adding plasticizers [8].

A recent work by Erin Koos et al. [9] provides a comprehensive state of art in the origin of crack formation and of the strategies to suppress cracks during drying.

From these considerations it is evident that a reliable experimental determination of the biaxial stress in the layer during drying is essential to understand the effect of the process parameters and avoid the formation of such cracks.

Several methods have been reported in literature to quantify the stress formation during drying and in relation with the kinetics of the solvent evaporation. One of them, the cantilever deflection method, has largely been used due to the simplicity of its concept and measurement apparatus [10-12]. Some recent works [13] show the possibility to measure the mass loss simultaneously with the development of planar stresses by the cantilever deflection method.

However, there are very few studies on the optimization of the cantilever's geometry, and the designs of cantilever reported in the literature are all quite similar, see Table 1, except for the design reported by A. Roosen et al. [13]. Indeed, this last work provides an interesting experimental development with a longer cantilever (110 mm length, differently from previous works with cantilevers of 40-50 mm in length). This cantilever design allows to increase the accuracy of the in-plane stress measurements during drying, but it requires to take into account the mass loss of solvent during drying, which can significantly impact the cantilever deflection.

References	Mechanical properties of cantilever		Geometry properties of cantilever			Properties of coating		Possibility of simultaneous measurements with mass loss
	Young Modulus E_s (GPa)	Poisson's ratio ν_s	Thickness h_s (mm)	Length L (mm)	Width b (mm)	Young Modulus E_c (GPa)	Final thickness h_s (mm)	
Lewis et al. (1996) [11]	170	0.27	0.3	40	6	n.c.	0.06 – 0.14	no
Payne et al. (1997) [10]	n.c.	n.c.	0.15-0.5	45	6	n.c.	n.c.	no
Wedin et al. (2005) [12]	190	0.36	0.24-0.4	50.8	6.38	n.c.	0.1-0.25	no
Kiennemann et al. (2005) [7]	200	0.29	0.2	50	5	10-12	0.15-0.25	no
A. Roosen et al. (2015) [13]	190	0.29	0.3	110	n.c. (10<)	n.c.	0.05-0.1	yes
E. Koos (2021) [14]	210	0.3	0.2	40	6	n.c.	0.25	yes

Table 1. Listing of cantilever parameters reported in previous works.

Our work investigates the optimal cantilever and apparatus design to achieve accurate measurements of the in-plane stress development during the drying of ceramic layers.

Combining analytical considerations and experimental evidence, it is shown that the design parameters should be optimized not only by considering systematic errors depending on the ratio between the layer's and substrate's stiffnesses, but also by minimizing measuring artifacts due to the inhomogeneous drying of the ceramic suspension. In particular, it is suggested that the cantilever design should be adapted to the properties of the ceramic slurry and of the resulting layer.

The optimized setup is finally tested by comparing the stress evolution and mass loss during drying of four alumina slurries with different particle size distributions, developed for the layerwise slurry deposition (LSD-print) additive manufacturing process. The simultaneous measurement of in-plane stress and mass loss supports the interpretation of the drying's mechanisms at different stages.

2. Materials and methods

2.1 Cantilever deflection method

The cantilever beam is made of stainless steel with Young modulus of 200 GPa and Poisson's ratio of 0.29, an effective length of 50, 75 mm or 135 mm, a width from 8 to 45 mm and various thickness from 0.1 to 0.5 mm. The shrinkage on the coating thickness and the beam deflection is measured using two laser displacement sensors (ILD1900-2**,** Micro-Epsilon, France), with an accuracy of +/- 2

µm. The displacement sensor can be affected by the tilt of the cantilever beam during the coating drying, as described in previous work [15]. In this work, this systematic error has been evaluated to be less than 0.3 microns and can then be neglected. Figure 1 shows the principle of the cantilever deflection method used in this work.

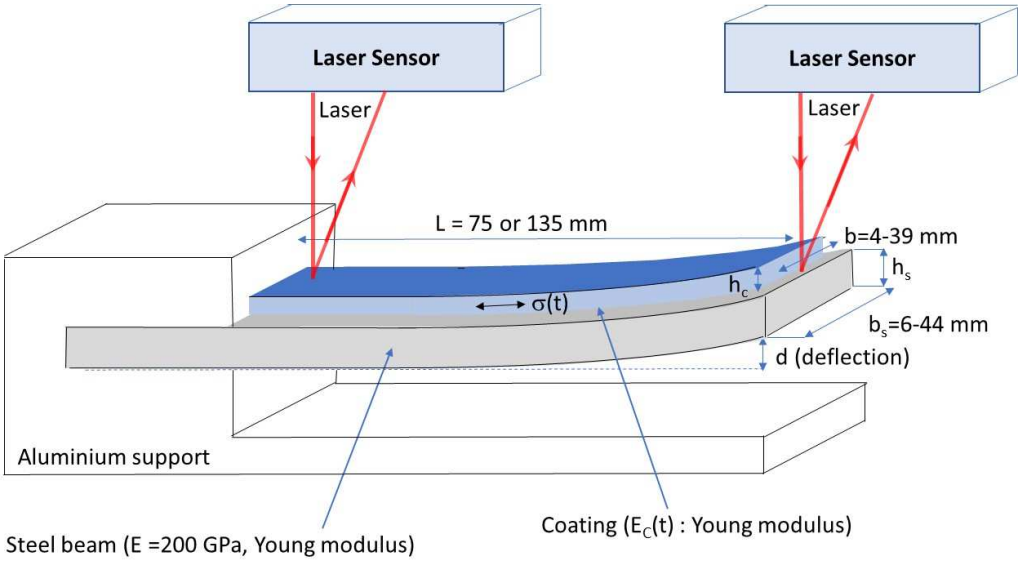

Figure 1. Scheme of cantilever deflection device, with the main mechanical and geometrical properties used for the determination of in-plane stresses developed during drying.

The cantilever device is positioned on an analytic balance (Entris II Essential, Sartorius, France, accuracy: 0.001 g, maximal mass 620 g). The originality of this setup is the possibility to measure simultaneous the mass loss, shrinkage and the in-plane stress development in the coating during drying.

The cantilever device and the analytic balance are located in a close chamber at 18°C and with the relative humidity close to 40 % using a water solution saturated by potassium carbonate salt [16].

The spreading of slurry on the cantilever beam is performed using the mini-tape caster and mini doctor blade shown in Figure 2, with a gap height of 0.3 mm and different widths of blade: 4, 8, 12, 39 mm in this work. The average speed of doctor blade is close to 20-25 $mm.s^{-1}$.

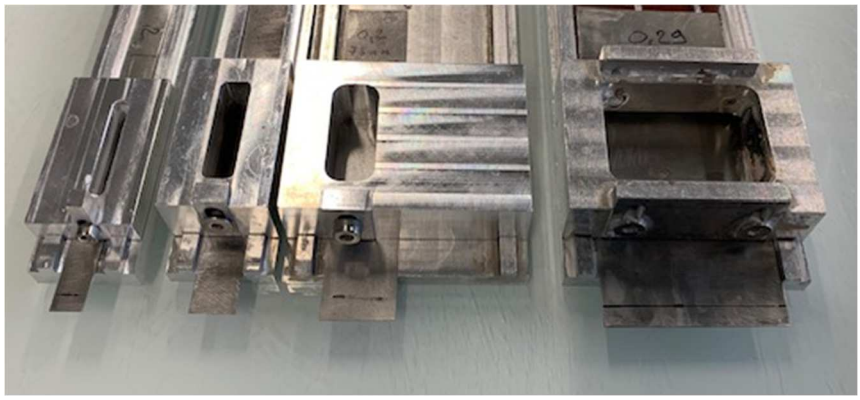

Figure 2. Mini-doctor blades with 4, 8, 12, 39 mm of blade width adapted to the spreading of slurry on the cantilever beams with 8.4, 11.7, 17.6, 44 mm of width, from the left to the right respectively.

To obtain a homogenous spreading of slurry on the cantilever, the technical solution required in this work is the use of a cantilever beam with slightly larger width (of 2-4mm) than the width of the coating (i.e. $b > b_s$, with b = the width of coating and b_s = the width of cantilever beam, see figure 1). Then, the doctor blade is lightly pressed directly on the cantilever during the spreading of slurry, which leads to obtain a homogenous thickness of coating on the beam.

2.2 Alumina powder characterization and slurry preparation

In this work, four alumina powders with different specific areas and particles sizes were used to formulate water-based slurries with hydroxymethyl cellulose (HEC) binder.

The particle size distribution was measured by laser diffraction method (Mastersizer 3000, Malvern Panalytical Ltd, UK) according to ISO 13320. The powder was dispersed in a 3 mmol/l $Na_4P_2O_7$ solution and sonication (Sonopuls HD4200) was applied to deagglomerate the dispersion. The specific surface area was measured by BET method (NOVA 2200, Quantachrome GmbH, Germany) with nitrogen gas.

Four alumina slurries were prepared with respectively the four powders listed in Table 2. All four slurries had the same nominal composition; thus, they are denominated based on the powder name in the following (CT3000, CT530, CT1200, Nabalox).

The composition of the slurries is shown in Table 2.

Components	Wt.%	Vol.%
Alumina powders (specific surface area): - CT3000 (5.9 $m^2.g^{-1}$) - CT530 (4.3 $m^2.g^{-1}$) - CT1200 (2.9 $m^2.g^{-1}$) - Nabalox (2.1 $m^2.g^{-1}$)	67.5	34.5
Water (deionized)	31.6	64.1
Hydroxyethylcellulose (HEC)	0.5	0.8
Dispersant (CE64)	0.4	0.6

Table 2. Composition of alumina slurries. All four slurries (CT3000, CT530, CT1200, Nabalox) have the same nominal composition.

The slurries were produced by first dissolving the hydroxyethylcellulose (HEC, Sigma-Aldrich, S7835968210) in deionized water. A homogeneous solution was obtained by mixing in a bottle with alumina milling balls (10.8 mm diameter) on a roller mixer for two hours.

The dispersant (Dolapix CE64, Zschimmer & Schwarz, Ch.: 228341001) and half of the alumina powder were then added and mixed in a tumbler mixer for 30 min. The rest of the alumina powder was then added, followed by 1 hour mixing in the tumbler mixer. Finally, the slurries were further mixed for 26 hours on a roller mixer for homogenization and degassing.

3. Theory and analysis of systematic errors

3.1 Corcoran's equation: relationship between in plane stresses and cantilever beam deflection

The Corcoran's equation [17] gives the analytic solution of the average in-plane stress (σ) developed in the coating as a function of time (t) in relation with the deflection of cantilever (d(t)):

$$\sigma(t) = \frac{d(t)\, E_s h_s^3}{3 h_c L^2 (h_c+h_s)(1-\nu_s)} + \frac{d(t)\, E_c(t)(h_c+h_s)}{L^2\,(1-\nu_c)} \qquad (2)$$

The cantilever has length L and thickness h_s, while the coating has thickness h_c and the same length L. E_s, E_c, ν_s and ν_c are the Young moduli and Poisson's ratios of the substrate and coating, respectively.

E_s corresponds to the effective Young modulus of a beam with the same width of the coating. In this work, the width of coating is lower than that of the cantilever, thus the effective modulus of the substrate corresponds to $E_s = b_s/b * E$ (with E: Young modulus of the steel beam, see complementary information S1 for more details). For instance, E_s= 320 GPa, if E= 200 GPa, b = 8 mm and b_s=11.7 mm.

The second term of the Corcoran's equation is often considered negligible, because $E_c(t)$ is usually very low in comparison to E_s. This approximation is often made because $E_c(t)$ is a function of the drying time and it is difficult to measure experimentally.

However, Kiennemann et al. [7] show that the second term in Corcoran's equation can be significant, and it must be considered in the determining in-plane stresses, in particular at the end of drying. In this same work, the Young modulus of the ceramic coating has also been measured by ultrasonic methods, resulting in a Young modulus close to 12 GPa at the end of the drying [7]. In the current study, the Young modulus of the alumina coatings has been estimated in the range 6-10 GPa at the end of drying, based on ultrasonic measurements of green alumina cylinders cast in a plaster mold. Thus, it should not be assumed that the second term of the Corcoran's equation is insignificant without further investigation.

The Corcoran's equation can be expressed as following in order to easily identify the key parameters which control the contribution of the second term.

$$\sigma(t) = \frac{d(t)\, E_s h_s^3}{3h_c L^2 (h_c+h_s)(1-\nu_s)} \left(1 + \frac{E_c(t)}{E_s} \frac{3h_c(h_c+h_s)^2}{h_s^3} \frac{(1-\nu_s)}{(1-\nu_c)}\right) \qquad (3)$$

The systematic error linked to the contribution of the second terms in Cororan's equation can be expressed as following:

$$\frac{\Delta\sigma(t)_{error}}{\sigma(t)} = \frac{E_c(t)}{E_s} \frac{3h_c(h_c+h_s)^2}{h_s^3} \frac{(1-\nu_s)}{(1-\nu_c)} \qquad (4)$$

Where

$\frac{E_c(t)}{E_s}$ corresponds to the impact of the cantilever's mechanical properties on the systematic error,

$\frac{3h_c(h_c+h_s)^2}{h_s^3}$ corresponds to the impact of the cantilever's geometry on the systematic error,

$\frac{(1-\nu_s)}{(1-\nu_c)}$ is very close to 1.

Figure 3 shows the relative and systematic error induced by second terms of Corcoran's equation in relation to the ratios $\frac{E_s}{E_c(t)}$ and $\frac{h_s}{h_c}$.

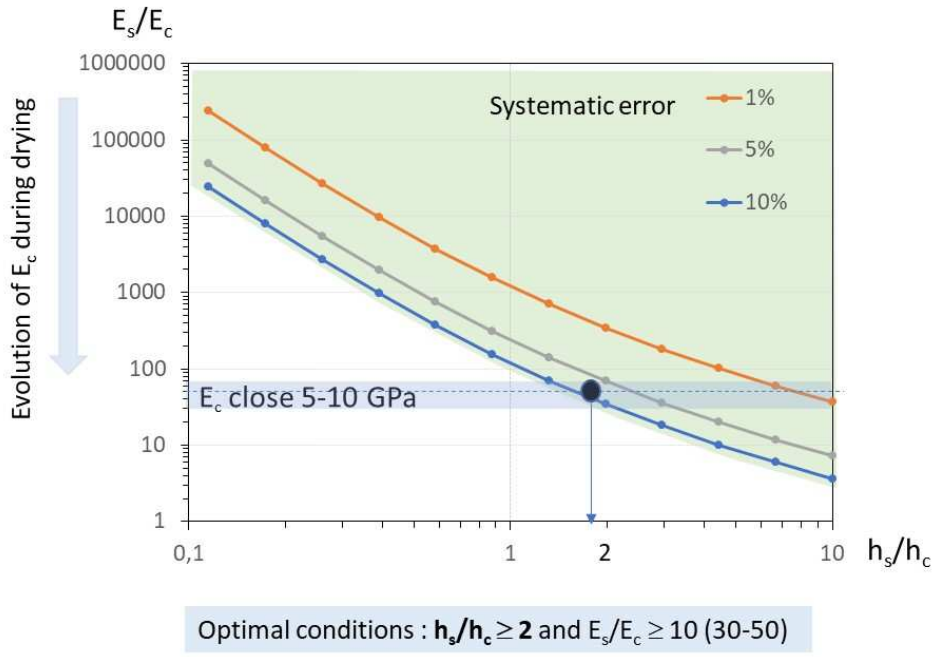

Figure 3. Impact of ratios $\frac{E_s}{E_c(t)}$ *and* $\frac{h_s}{h_c}$ *on the systemic error linked to the second terms of Corcoran's equation.*

From Figure 3 it can be noted that the thickness and Young modulus of cantilever must be significantly larger than those of the coating during drying. It is worth of note that the Young modulus $E_c(t)$ is a function of the drying time. In a typical experiment, $E_c(t)$ is negligible at the beginning (since the coating is still in a viscous state) and it increases up to a maximum value during drying. Considering a final E_c in the order of 10 GPa in this work, the conditions $h_s/h_c \geq 2$ or $E_s/E_c \geq 30$ should be met to limit the systematic error at 10 %. On one hand, a large h_s decreases the magnitude of the cantilever deflection, introducing a larger relative error in the measurement of deflection d(t). On the other hand, a small h_c can cause difficulties to obtain experimentally a homogeneous thickness and moderate drying kinetics.

The data reported in Table 1 show that the thickness of coating (h_c) is usually close to 0.1-0.2 mm in the literature, because this range of thickness corresponds to a best compromise between a decreasing of the coating thickness to decrease the second terms of Corcoran's equation, and a suitable thickness to obtain a homogeneous slurry distribution.

3.2. Effect of mass loss during on cantilever deflection

A solution to increase the magnitude of the cantilever deflection while maintaining a large thickness ratio ($h_s/h_c \geq 2$) is to use a longer cantilever (L > 50 mm).

Unfortunately, this requires to take into account the mass loss during drying. The contribution of the cantilever deflection due to the mass loss during drying is calculated using the general formula of beam deflection, equation 5.

$$d_m = \frac{1}{8}\frac{\Delta w L^4}{E_s I} \quad (5)$$

where Δw is the change in distributed load and I is the moment of inertia.

Substituting $\Delta w = \frac{\Delta m\, g}{L}$ (Δm is the change in slurry mass, g is the gravitational acceleration) and $I = \frac{b\, h_s^{\,3}}{12}$, equation 6 is obtained.

$$d_m(t) \approx \frac{1.5*9.8*L^3}{E_s b h_s^{\,3}} \quad (6)$$

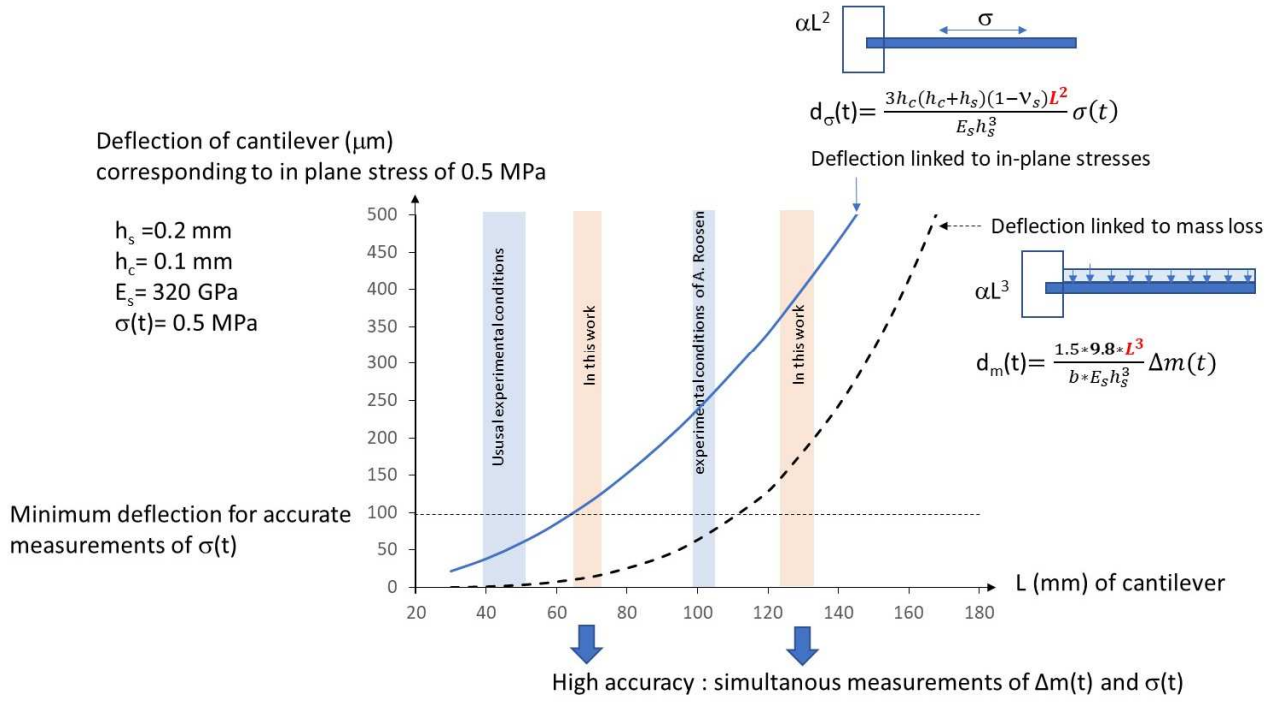

Figure 4. Impact of cantilever length on the deflection linked to the in-planar stress development and the mass loss linked to solvent evaporation during drying.

Then, in an accurate cantilever setup, the mass loss must be simultaneously measured with the cantilever deflection, as reported by A. Roosen. It is likely for these reasons that the results obtained by Roosen et al. show more accurate data of stress development during drying in comparison to the previous works, see figure 4.

However, the large deflection linked to the mass loss of solvent during drying can lead to significantly decreasing the accuracy of the deflection measurements linked to the in-planar stresses in the coating, in particular for L >160 mm (Figure 4, with a large deflection linked to mass loss > 300 µm).

It is also necessary to limit the deflection linked to the mass loss of solvent in comparison with the deflection linked to the in-plane stresses in the coating.

Figure 5 shows the mapping of beam deflection as a function of the thickness and length of cantilever with $h_s/ h_c= 2$. It is noted that the optimal length of the cantilever beam depends on the magnitude of beam deflection and also on the values of in-plane stress. The laser sensors typically have a measuring range of maximum 1 mm. Thus, it is considered optimal to achieve a deflection > 100 µm and close to the maximum of 1 mm. The conditions are given as (i) $h_s > 100$ µm, to avoid mechanical instability of the substrate, like vibrations, and (ii) $h_c = 100$ µm, which is necessary to achieve a homogeneous coating and to obtain a suitable drying time, higher than 10-20 minutes.

In case of LSD or tape casting slurries, the maximum of in-plane stresses in the coating is usually close to 0.3-1 MPa in the literature. In this case, the optimal design of cantilever beam corresponds to a length of 70-150 mm and thickness of 0.1-0.4 mm.

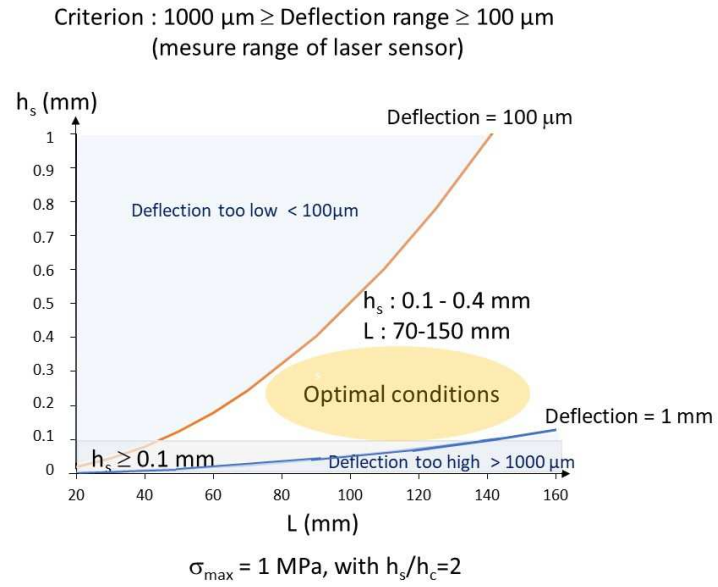

Figure 5. Determination of optimal length and thickness of the cantilever beam in agreement with the deflection range of the laser sensor.

4. Results and discussion

4.1 Impact of cantilever dimensions on the accuracy of in-plane stress measurements in the coating during drying

The influence of the cantilever's geometrical parameters on the evolution of in-plane stresses during drying has been experimentally studied in this section. A particular attention is paid to the influence of the cantilever width, thickness and the length. In the following sections 4.1.1, 4.1.2 and 4.1.3, the

results shown use the same slurry formulation using CT3000 alumina powder, as reported in section 2.2.

4.1.1 *Influence of the cantilever width (d) on the measurements of in-plane stress in the coating during drying*

While the effect of the cantilever thickness can be discussed from a theoretical point of view as in section 3, the influence of the cantilever width on the accuracy of the in-plane stress measurements in the coating during drying is more difficult to model. For this reason, this is usually not discussed in the literature and the width is often set arbitrarily close to 6 mm (see table 1). Figure 6 shows the influence of the cantilever width (with b_s= 8.4, 11, 17, 44 mm which must be associated here to the coating width with b= 4, 8, 12, 39 mm, respectively) on the development of the average in-planar stresses in the coating during drying. It is clearly noticeable for b > 15-20 mm, that the maximum of stress peak decreases and the peak broadens when the cantilever width increases. This trend gives evidence of the inhomogeneous drying kinetic between the edge and the center of the coating, which increases with the coating width (b), in particular when b > 15-20 mm.

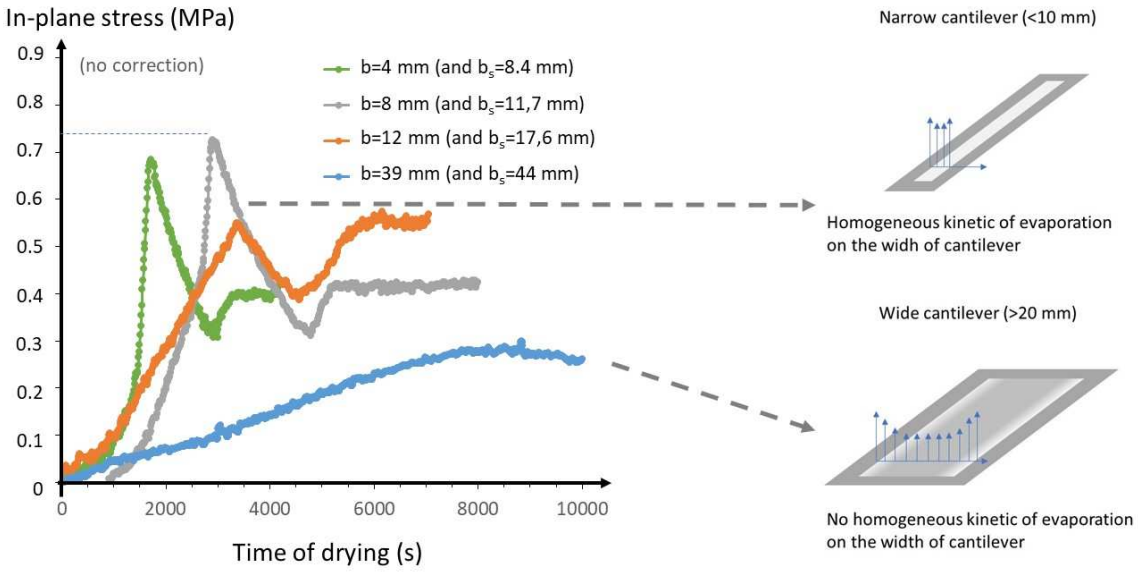

Figure 6. Influence of cantilever width (without mass loss correction) on the values of in-plane stress measurements, with cantilever length of 75 mm and thickness of 0.2 mm. In this study, the slurry formulation is based on the CT3000 alumina powder, as described in the section 2.2.

The maximum of in plane-stresses is delayed when the coating width is larger, which is linked to lower kinetic of evaporation on the coating's center (see table 3). Then, there is here evidence that the coating drying is not homogenous on its surface, in particular between the edge and the center. The inhomogeneous evaporation rate at the coating's surface had already been observed by Roosen [13] and it is often reported in the literature as "coffee ring" effect for the drying of suspension drops

[18], or as “lateral drying” which is observed in case of drying coatings on large surfaces [19-21]. Accordingly, Xiao et al. [21] and Lewis et al. [20] reported that the evaporation rate at the coating’s surface is higher at the coating edge in comparison to the center.

Besides, the simultaneous measurements of mass loss during drying leads to define a best compromise between a suitable accuracy of the weight loss measurement and a good accuracy of in-plane stress measurements in the coating during drying. This compromise is found here with a cantilever width of 8 mm, as reported in the Table 3, which is a good agreement with the experimental conditions reported in previous works (see Table 1).

Width of coating (b) in mm	Maximum of in-plane stresses (MPa)	Drying time to reach the maximum of in-plane stress: t_{max} (s)	Time total of drying (s)	Mass of coating in g (at t=0 s)	Relative Error of mass loss
4	0.7	1800	3000	0.162	+/- 1.3%
8	**0.73**	**3000**	**4900**	**0.338**	**+/- 0.6%**
12	0.55	3500	5300	0.535	+/- 0.4%
39	0.29	8200	18000	1.997	+/- 0.1%

Table 3. Influence of coating width on the drying time, the maximum of in plane stress and the systematic error linked to mass loss during drying.

4.1.2 *Influence of cantilever thickness (h_s) on the measurements of in-plane stress in the coating during drying*

In this section, a comparative study is performed with various cantilever thicknesses: 0.1, 0.2, 0.3, 0.4, 0.5 mm, which corresponds to ratios h_s/h_c = 0.5, 1, 1.5, 2, 2.5 respectively (with h_c=0.2 mm).

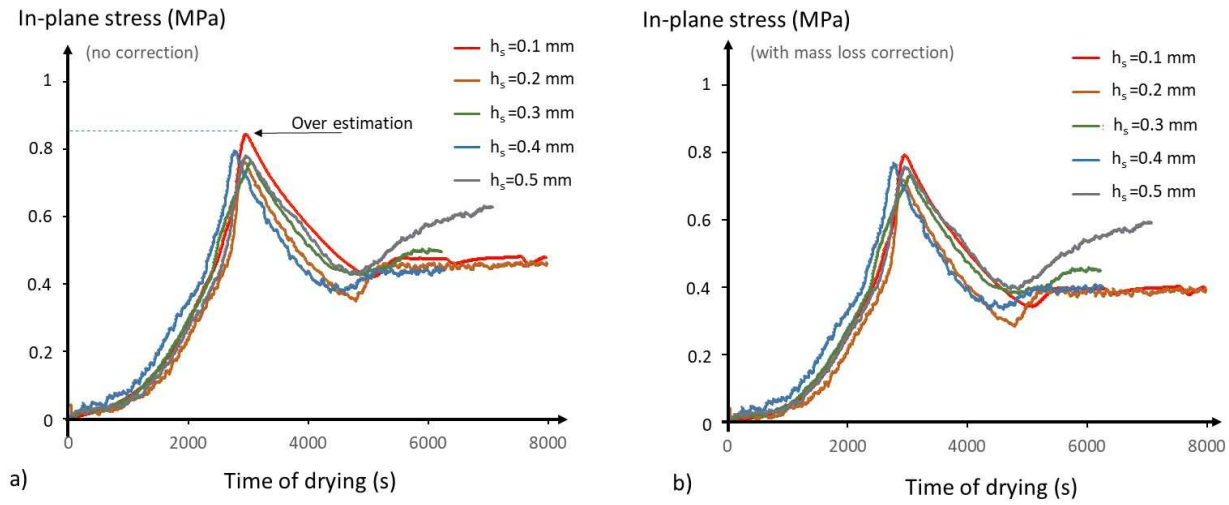

Figure 7. a) Influence of cantilever thickness without correction and b) with the mass loss correction on the values of in-planar stress measurements, with cantilever length of 75 mm. In this study, the slurry formulation is based on the CT3000 alumina powder, as described in the section 2.2.

Figure 7 shows the evolution of in-plane stress measured in the coating during drying with and without mass loss correction and with various thickness of cantilever (h_s = 0.1, 0.2, 0.3, 0.4 and 0.5 mm), with constant h_c = 0.2 mm. It can be noted that the evolution and the maximum values of in-plane stress during drying are very similar independently of the cantilever thickness. However, there is a slight overestimate of the in-plane stress if the cantilever deflection linked to mass loss due to water evaporation during the drying is not considered (see Figure 7 b, with mass loss correction). This result gives evidence that the second term of Corcoran equation can be neglected in this work, although the ratio h_s/h_c varies from 0.5 to 2.5. This suggests that the Young modulus of the coating during drying remains low (1-5 GPa).

It also is noticeable that the intensity of the in-plane stress increases until a maximum close to 7.5 MPa during the first step of drying, and decreases until reaching a stable value corresponding to the residual internal stress after drying. These values of residual internal stress after drying are also similar independent the cantilever thickness, except for the largest cantilever thickness (h_s=0.5 mm) corresponding to high rigidity of cantilever.

4.1.3 *Influence of cantilever length (L) on the measurements of in-plane stress during drying*

Figure 8 shows the evolution of in-plane stress in the coating during drying with various cantilever length (L= 50, 75, and 135 mm) and various cantilever thickness (h_s=0.2, h_s=0.3 and h_s=0.4 mm). The values of the in-plane stress measured with the shortest cantilever beam (L=50mm) are significantly underestimated (maximal stresses are 0.4-0.5 MPa and not 0.7 MPa as expected) in comparison to the values obtained with a longer cantilever beam. The evolution of in-plane stress obtained with L= 75 mm and L= 135 mm is instead similar. Indeed, this trend is likely linked to the homogeneity of the kinetic of drying on the coating's surface. In the case of a short cantilever beam (L < 8b), the higher kinetic of evaporation of water on the extremity of cantilever has a large impact on the average evolution of in-plane stress in the coating, and this impact decrease when the length of cantilever increases, in particular when (L>8·b, which is the case for L= 75mm or 135 mm). The kinetic of the stress evolution supports this hypothesis: the peak of in-plane stress in the coating occurs earlier with L=50mm during the drying (t= 2500 s) compared to L= 75 mm and L= 135 mm (t= 3000 s).

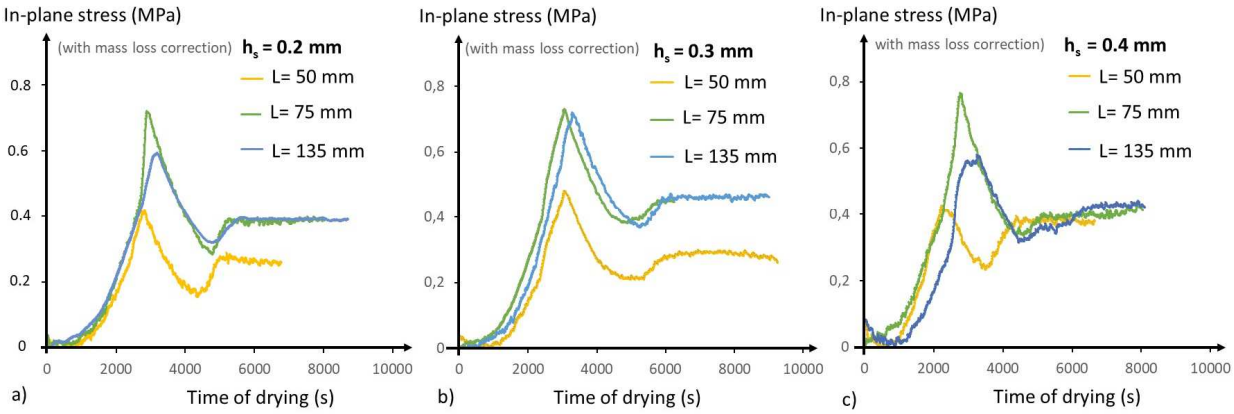

Figure 8. Influence of cantilever length on the values of in-planar stress measurements during the drying with a) h_s= 0.2, b) h_s= 0.3 and c) h_s= 0.4 mm. In this study, the slurry formulation is based on the CT3000 alumina powder, as described in the section 2.2.

The results of section 4.1.1 highlight that the homogeneity of drying has a significant effect on the accuracy and reproducibility of the stress evaluation. An inhomogeneous drying in the coating can lead to a significant underestimation of the drying stresses, in particular if the cantilever is too short or too wide. This confirms that the cantilever method can be an accurate technique to measure the low intensity of in-plane stresses in coating during drying, but it is very important to define the experimental conditions which lead to a homogeneous coating thickness and homogeneous water evaporation kinetics.

To conclude, the optimal conditions correspond here to a large length of cantilever L=75 or 135 mm with thickness of 0.2 or 0.3 mm. However, we recommend here a cantilever length close to 75 mm to limit the erratic vibrations of cantilever linked to possible environmental perturbations.

It is important to highlight here that these conditions must be optimized experimentally for each type of material and slurry system. At least in the frame of the current study, it is not possible to derive a simple model only starting from Corcoran's theory, because Corcoran's model assumes the homogeneous drying of the coating.

4.2 Study of in-plane stress development during drying for LSD-print slurries

4.2.1 Powder characterization

The characteristics of the starting alumina powder are presented in Table 4.

Powders	BET specific surface area ($m^2.g^{-1}$)	$D_{V,10}$ (µm)	$D_{V,50}$ (µm)	$D_{V,90}$ (µm)	Providers
CT3000	5.9	0.2	0.5	3.1	Almatis, Germany
CT530	4.3	0.4	2.2	6.3	Almatis, Germany
CT1200	2.9	0.9	1.8	3.5	Almatis, Germany
Nabalox NO-725-10	2.1	1.3	2.6	4.6	Nabaltec, Germany

Table 4. Characteristics of starting alumina powders.

The results confirm that the BET specific surface area decreases from CT3000, CT530, CT1200 to the Nabalox powder. CT530 and CT1200 showed similar $d_{V,50}$ values, but with a wider particle size distribution for CT530 compared to CT1200. The reason for this difference is that CT530 has a bimodal distribution (peaks at approx. 0.5 µm and 3 µm, see Supplementary Information S2: granulometry distribution of alumina powders), while CT1200 is monomodal.

4.2.2 Evolution of in-plane stress during drying

Using the optimized experimental conditions determined in section 4.1, Figure 9 shows the in-plane stress development, mass loss linked to water evaporation, and shrinkage during drying of an alumina (CT3000) coating. The evolution of the stress can be divided mainly in 4 steps of drying, and these 4 steps are also observed for all suspensions studied in this work, as presented in the next section. These four steps of drying can be interpreted as following:

1) During the first step of drying, the evaporation rate and the shrinkage rate on the coating thickness are constant. This step is generally denominated constant rate period (CRP) [1].
   The coating corresponds to suspension (solid/liquid) where the ceramic particles still have large mobility and do not form a compact granular structure yet.

   This stage corresponds to a ratio (Volume of water / initial volume of suspension) >29%, see figure 9.

2) The second step of drying [1] starts with the end of shrinkage (on the coating thickness), and with the increasing of in-plane stress. At this stage, the in-plane stress increases due to the formation of water bridges between particles, while the microstructure gradually evolves from a capillary state to a funicular state. At the same time, the drying rate decreases in the falling rate period (FRP), because the transport of water is limited by the diffusion kinetics from the bulk to the surface.
   This stage corresponds to a ratio (29% > Volume of water / initial volume of suspension > 24%) see figure 9.

3) The third step of drying starts here when the in-plane stress and capillary stress between particles decreases, corresponding to the emptying of the capillaries and the evolution of the microstructure from the funicular stage towards a pendular bridge stage in the granular compact, and then the progressive reduction of water bridges between particles.
   This stage corresponds to a ratio (24% > Volume of water / initial volume of suspension > 2%), see figure 9.

4) The last step corresponds to a second increase of the in-plane stress. This stage may seem unexpected, since it is not described in the general theory of drying of granular bodies. However, it should be considered that the slurry used contains HEC as a binder dissolved in the liquid phase. When the residual water is removed, this leads to an increase of the rigidity of the polymer bridges binding the ceramic particles, resulting in an increase of stress in the layer. Indeed, it is likely that the residual water (1-2 wt% at this stage) plays the role of a plasticizer for the HEC binder. It can also be noted that the drying rate becomes very low at this point. The remaining water (< 1 wt%) is indeed expected to slowly reach an equilibrium between the atmosphere, the hydrophilic polymer, and the surface of the particles.

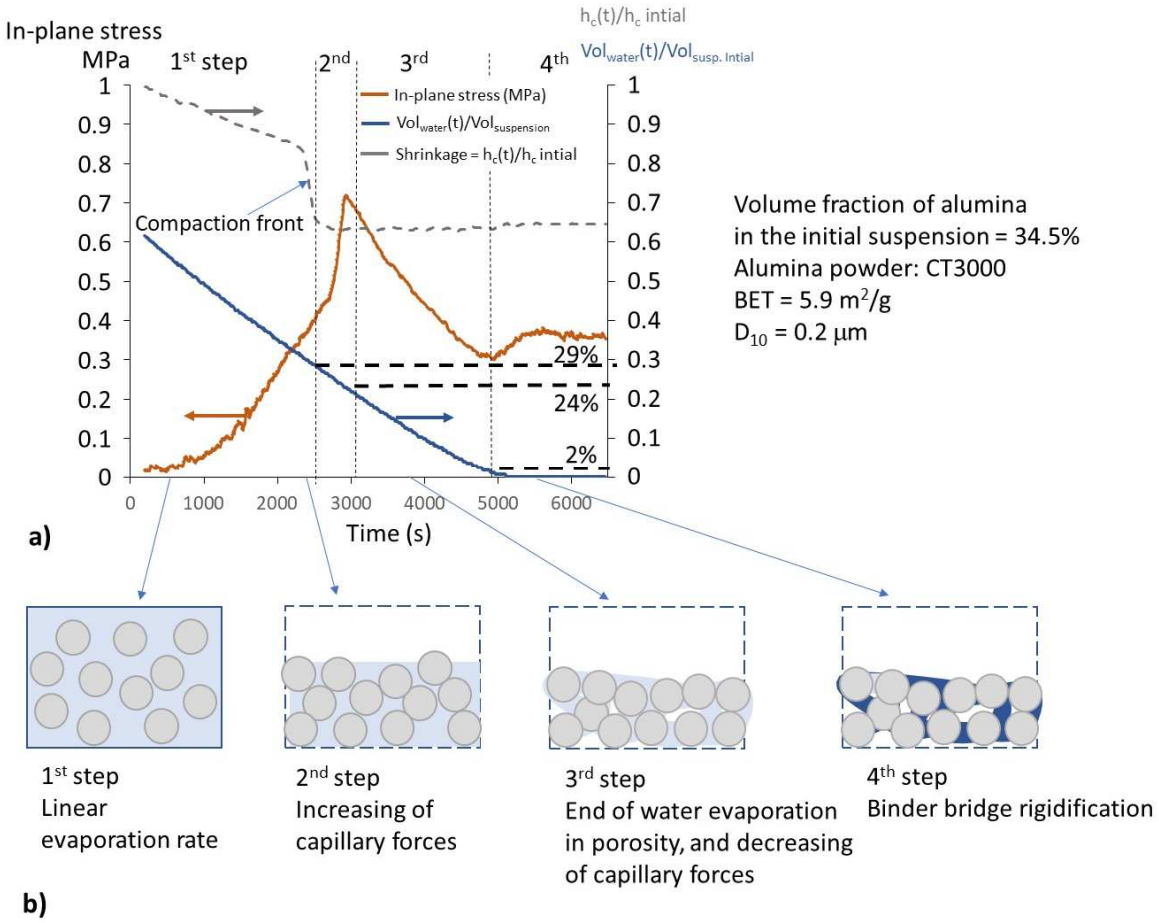

Figure 9. a) Evolution of shrinkage and in-plane stress during drying of a CT3000 alumina coating, with L=75 mm and h_s=0.2 mm, and b) four stages of coating drying.

This evolution of in-plane stress during drying in four steps, as described in figure 9, is very similar to the results reported previously by Lewis et al. with colloidal silica suspensions using the optical interference method [15]. In Figure 9, the maximal stress at the end of the 2nd step of drying of CT3000 alumina coating is close to 0.7 MPa. This value is higher than the maximal stress reported in the literature by Chartier or Roosen, from 0.3 MPa to 0.6 MPa, for aqueous alumina suspension for tape casting process (with larger ratio of binder, 10 to 12 % in weight of CT3000 SG alumina powder [13]). However, the stress magnitude is similar to the values reported by Lewis et al (0.6-1 MPa) with colloidal silica suspensions.

In the current study, a large relative shrinkage on the coating thickness (close to -35%) is observed, while Chartier et al. have reported a final relative shrinkage close to -16%. This is likely linked to the low binder content and low solids content of the suspension used in this work, which is favorable to the reorganization of particles at the end first step of drying. Interestingly, this results in a densely

packed layer with a significantly lower volume of water at the end of the first stage of drying compared to previous work reported by Chartier and Roosen.

The large variation of shrinkage observed at the end of the first stage of drying corresponds to the passage of the compaction front below the laser sensor, which can be described as a local evolution of the coating from supersaturated to saturated zone (see figure 9). This phenomenon is also observed during the drying of suspensions with low binder content and is described in the literature [21-23] and more recently by Nassa [24]. This however shows clearly one of limit of this setup which measures the variation in thickness on a single point (spot of the laser sensor). As a result, the shrinkage measurement corresponds to the local variation of coating thickness (supplementary information: S3) and not to the average variation of coating thickness. Then, the relative final shrinkage is not exactly same on the center on ledge of coating, as is usually observed on the drying of ceramic suspensions in the literature [25]. The shrinkage measurements should therefore be interpreted with caution when visualized together with the weight loss and in-plane stress measurements, because the latter two are instead values which are averaged on the whole coating surface, while the shrinkage measurements correspond to the local evolution on the coating surface.

For this reason, it is more meaningful to evaluate quantitatively the water ratio in the coating, rather than the shrinkage. At the end of the first drying stage, the water ratio is close to 29 vol% of the initial volume of suspension. This corresponds to a fraction of 45 vol% water in the coating, i.e., 55 vol% packing density of particles in the water-saturated coating. At the end of the second stage, the fraction of water decreases to 40 vol% as the pores start to empty.

These values are consistent with the description of a compact granular structure when the ceramic particles are in contact and the residual porosity is saturated in water (see figure 9b). This description also suggests that the impact of powder granulometry and packing density likely have a large impact on the ratio of water at the end of the first drying stage. This aspect will be investigated in the next section 4.2.3.

4.2.3 Influence of the granulometry of starting alumina powder on the maximum and the evolution of the in-plane stresses during the drying

Figure 10 shows the shrinkage, the weight loss and the in-plane stress development during the coating drying obtained with four different alumina powders of four different powder granulometries. The main data collected from Figure 10 is reported in Table 5. The coating drying obtained with four alumina suspensions can be described in the four main steps in Figure 9, as described in section 4.2.2, and the data collected in Table 5 gives evidence on the impact of capillary

stress intensity on the in-plane stress during the coating drying. For instance, the maximal in-plane stress is 7.1 MPa with CT3000 powder (BET= 5.9 m^2/g), while the maximal in-plane stress is only 1.1 MPa with Nabalox alumina powder, BET= 2.1 m^2/g). A dependence of the fine powder ratio (corresponding to the value of D_{10}) on the intensity of in-plane stress can also be observed.

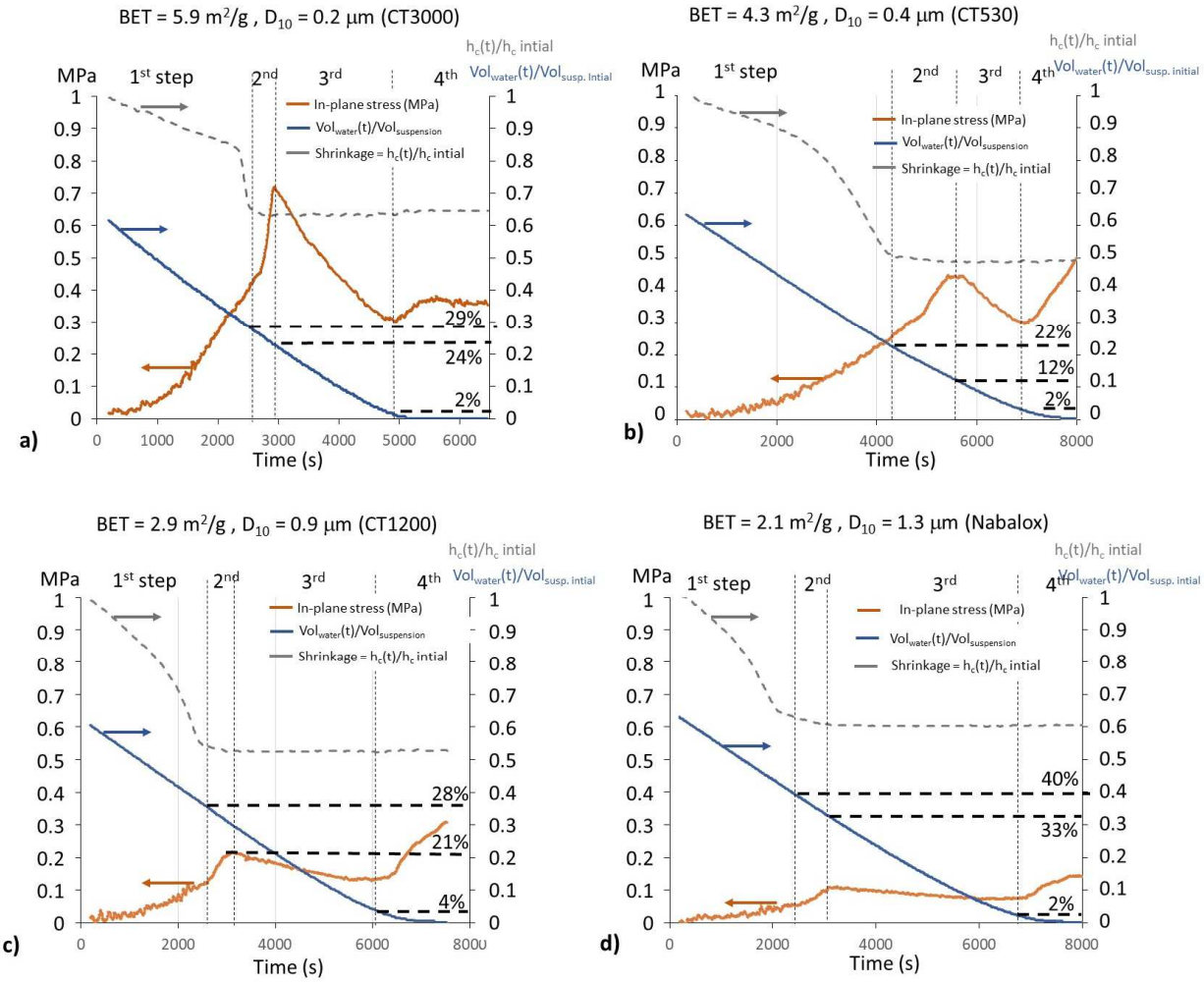

Figure 10. Influence of powder granulometry on the evolution of shrinkage, weight loss and in-plane stress during drying, with L=75 mm and h_s=0.2 mm. a) alumina powder with BET = 5.9 $m^2.g^{-1}$ (CT3000 SG), b) with BET = 4.3 $m^2.g^{-1}$ (CT530), c) with BET = 2.9 $m^2.g^{-1}$ (CT1200),with BET= 2.1 $m^2.g^{-1}$ (CT530).

Powders	BET ($m^2.g^{-1}$)	D_{10} (µm)	D_{50} (µm)	D_{90} (µm)	Intensity of peak stress (MPa)	Packing density of coating (1)	Porosity of coating (2)	Ratio of $Vol_{water}/Vol_{susp.}$ at the end of 1st drying step (3)	Ratio of Vol_{water} / $Vol_{sup.\ intial}$		
									at the end of 1st drying step	at the end of 2rd drying step	at the end of 3rd drying step
CT3000	5.9	0.2	0.5	3.1	7.1	55%	**45%**	**45%**	29%	24%	2%
CT530	4.3	0.4	2.2	6.3	4.5	60%	**40%**	**38%**	22%	12%	2%
CT1200	2.9	0.9	1.8	3.5	2.1	53%	**47%**	**44%**	28%	21%	4%

Nabalox NO-725-10	2.1	1.3	2.6	4.6	1.1	44%	**56%**	**53%**	40%	33%	2%

(1) The packing density of the coating, P, has been evaluated from mass, width, length, and average thickness of coating after drying.

(2) The porosity ratio in the coating after drying = 1-P

(3) The ratio $Vol_{water}/Vol_{susp.}$ corresponds to the ratio between the volume of water and volume of suspension or coating = $(Vol_{water}/Vol_{sup.\ intial})/(0.36 + Vol_{water}/Vol_{sup.\ intial})$ with 0.36 corresponds to solid volume / initial suspension volume.

Table 5: Characteristics of the starting alumina powders and the parameter collected from figure 10 during the drying of the alumina coatings.

The initial ratios of water volume ($Vol_{water}/Vol_{susp.}$) in the coating are very similar for four alumina suspension coatings, i.e. close to 64% in Figure 10. This is expected since, the volume ratio of alumina powder is 34.5%, and the volume of organics is 1.4% in the initial alumina suspension. However, Table 2 clearly shows that the volume ratio of water at the end of first and second steps of drying depends strongly on the granulometry of alumina powder, ranging from 22 vol% of water to 40 vol% at the end of first step of drying and from 12 to 33 vol% at the end of second step of drying.

If the coating at the end of first drying step can be associated to a compact granular system where the porosity is saturated by water (see figure 10b), then the ratio of water volume at the end of first drying step must approximately correspond to the porosity ratio in the coating after drying. In this way, the values reported in Table 5 confirm this relationship between the water volume ratio and of porosity at the end of the first drying step.

The main consequence is also that the particle size distribution of the starting alumina powder (and not only the average particle size) has a large effect on the shrinkage and on the powder packing during drying. For instance, the powder CT530 shows the highest final packing density (60%) after drying, and correspondently the coating obtained with this starting powder leads to the lowest volume ratio of water ($Vol_{water}/Vol_{susp.\ intial}$= 22%) at the end of the first drying step, and ($Vol_{water}/Vol_{susp.\ intial}$= 12%) at the end of the second drying step. On the contrary, the CT1200 and Nabalox powders have similar D_{50} but lower packing density (53% and 44% respectively) compared to CT530 powder. These powders also lead to higher water volume ratios ($Vol_{water}/Vol_{susp.\ intial}$= 28% and 40%) at the end the first drying step, and ($Vol_{water}/Vol_{susp.\ intial}$= 21% and 33%) at the end of the second drying step.

Finally, also the evolution of in-plane stress during the second drying step is affected by the granulometry distribution of alumina powder. The second drying step for the CT530 coating is significantly longer, close to 1500 s in opposition to around 500 s for CT1200, CT3000 or Nabalox coatings (Figure 10), also corresponding to a large variation of water content in the coating ($Vol_{water}/Vol_{susp.\ intial}$ varies from 22% to 12% during the second drying step).

These results suggest that a wide granulometry of the starting powder can provide some advantages to prevent cracking during the coating drying, because wide distribution of particles size is favorable to on one hand obtain a compact and cohesive granular medium at the end of drying, and on other hand to have a broader peak of in-plane stress distributed on a larger time of drying. The wider granulometry distribution of particle sizes leads in particular to a longer second stage of drying, when the in-plane stresses in the coating increase quickly.

Conclusions

The cantilever design has a large impact on the accuracy of the in-planar stress measurements during the drying of wet ceramic coatings. This work shows in particular that the width of the cantilever must be low, typically close to 4-8 mm, to obtain an optimal estimation of the in-plane stress measurements. This trend is linked mainly to the large variation of water evaporation kinetics on the coating's surface, between its corner and the center.

This could be partially obtained in the following conditions, which however need to be optimized experimentally for each slurry system:

- Low width (w) of coating or coating: w **close to 4-8 mm**
- Large length of cantilever: **$L \geq 10w$**

In other way, the accurate measurement involves adapting the thickness and length of cantilever in relation with the maximal intensity of in-plane stress during drying.

This study was focused on slurries used for the layerwise slurry deposition process (LSD-print), which show a maximum of in-plane stress (< 1 MPa) which is same order of magnitude for slurries adapted for the tape casting process. Consequently, the optimal thickness of the cantilever depends on the nature of the suspension, which result in different elastic properties of the coating. In this work, we suggest also:

- **$L \geq$ 70 mm**
- **h_s = 0.2 mm** for slurries with low ratio of additive organics (used for the layerwise slurry deposition process) and hs= 0.3-0.4 mm for the slurries with large ratio of additive organics (used e.g. for tape casting)

The cantilever method combined with the measurement of mass loss and shrinkage was used to identify 4 steps during the drying of layers made from LSD-print slurries, and led to a better understanding of the stages of drying. In particular, a compaction front was observed at the end of the 1st drying step, which can be associated to the partial re-organization of particles linked to the

lateral capillary flows in the coating. Noticeably, this step of re-organization of particles is not observed with tape casting slurries and in slurries with large particles, likely due to the low mobility of particles in the compact granular structure. This work confirms that the drying conditions and granulometry of powder have a large impact on the final relative packing density of the coating after drying and that the granulometry distribution also has significant impact on the development of in-plane stress. The cantilever method presented in this work can largely be exploited to investigate other systems, such as tape casting suspensions, and provides useful information to identify the different steps or mechanisms which occur during the drying of cast ceramic layers.

References

[1] G. W. Scherer, Theory of Drying, Journal of American Ceramic Society 73 (1) (1990), 3-14. doi:10.1111/j.1151-2916.1990.tb05082.x

[2] Cima, M. J., et al. "Slurry-based 3DP and fine ceramic components." (2001).

[3] P. Lima, A. Zocca, W. Acchar, J. Günster, 3D printing of porcelain by layerwise slurry deposition, Journal of the European Ceramic Society 38(9) (2018) 3395-3400.

[4] A. Zocca, P. Lima, J. Günster, LSD-based 3D printing of alumina ceramics, Journal of ceramic science and technology 8(1) (2017) 141-148.

[5] Hu, M. S., Michael D. Thouless, and Anthony G. Evans. "The decohesion of thin films from brittle substrates." *Acta Metallurgica* 36.5 (1988): 1301-1307.

[6] Singh, Karnail B., and Mahesh S. Tirumkudulu. "Cracking in drying colloidal films." *Physical review letters* 98.21 (2007): 218302.

[7] J. Kiennemann, T. Chartier, C. Pagnoux, J. F. Baumard, M. Huger, J. M. Lamérant, Drying mechanisms and stress development in aqueous alumina tape casting, Journal of the European Ceramic Society 25 (2005) 1551{1564. doi:10.
1016/j.jeurceramsoc.2004.05.028.

[8] R. Belon, R. Boulesteix, P.-M. Geffroy, T. Chartier, L. Chretien, A. Maitre, Tape casting of multilayer YAG-Nd:YAG transparent ceramics for laser applications: study of green tapes properties, *Journal of European Ceramic Society,* 39(6), (2019) 2161-2167

[9] M. Schneider, J. Maurath, S. B. Fischer, M. Weiß, N. Willenbacher, and Erin Koos, Suppressing Crack Formation in Particulate Systems by Utilizing Capillary Forces, ACS Applied Materials Interfaces, 9 (2017) 11095−11105

[10] J. A. Payne, A. V. McCormick, L. F. Francis, In situ stress measurement apparatus for liquid applied coatings, Review of Scientific Instruments 68 (1997) 4564{4568.doi:10.1063/1.1148432.

[11] J. A. Lewis, K. A. Blackman, A. L. Ogden, J. Payne, L. F. Francis, Rheological Property and Stress Development during Drying of Tape-Cast Ceramic layers, Journal of American Ceramic Society, 79 (12) (1996) 3225-3234

[12] P. Wedin, C. J. Martinez, J. A. Lewis, J. Daicic, L. Bergstrom, Stress development during drying of calcium carbonate suspensions containing carboxymethylcellulose and latex particles, Journal of colloid and interface science 272 (2004) 1{9. doi:10.1016/j.jcis.2003.12.030.

[13] Z. Fu, U. Eckstein, A. Dellert, A. Roosen, In situ study of mass loss, shrinkage and stress development during drying of cast colloidal _lms, Journal of the European Ceramic Society 35 (2015) 2883{2893. doi:10.1016/j.jeurceramsoc.2015.03.029.

[14] S. B. Fischer, E. Koos, Influence of drying conditions on the stress and weight development of capillary suspensions, Soft Condensed Matter, arXiv:2009.08149v3 [cond-mat.soft] 10 Nov 2020.

[15] S. Li, Y. Yang, X. Jia, M. Chen, the impact and compensation of tilt factors upon the surface measurement error, Optik, 127 (2016) 7367-7373.

[16] L. Greenspan, Humidity Fixed Points of Binary Saturated Aqueous Solutions, Journal Of Research of the National Bureau of Standards - A. Phys ics and Chemistry, 81 A (1977) 1 , 89-96.

[17] E. M. Corcoran, Determining stresses in organic coatings using plate beam deflection, Journal of Paint Technology 41 (1969) 635-640.

[18] R.D. Deegan, O. Bakajin, T. F. Dupont, G. Huber, S. R. Nagel, T. A. Witten, Capillary flow as the cause of ring stains from dried liquid drops, Nature, vol. 389 (1997) 827-829.

[19] M. Suzuki, S. Maeda, On the mechanism of drying of granular beds, Journal of Chemical Engineering of Japan, (1967), vol. 1, 1, 26-31.

[20] J. J. Guo, J. Lewis, Aggregation effects on the compressive flow properties and drying behavior of colloidal silica suspensions, J. Am. Ceram. Soc., 82 (1999), 2345-2358.

[21] W. Lan, P. Xiao, Constrained drying of aqueous Yttria-Stabilized slurry on a substrate I/ Mechanism, J. Am. Ceram. Soc., 89 (2006), 1518-1522.

[22] W. Lan, P. Xiao, Constrained drying of aqueous yttria stabilized zirconia slurry on a substrate I: Drying Mechanism, J. Am. Ceram. Soc. 89 (2006) 1518-1522.

[23] D.H. Holmes, R. Vasant Kumar, W.J. Clegg, Cracking during lateral drying of alumina suspensions, J. Am. Ceram. Soc., 89 (2006), 1908-1913.

[24] M. Nassar, A. Gromer, D. Favier, F. Thalmann, P. Hébraud, Y. Holl, Horizontal drying fronts in films of colloidal dispersions: influence of hydrostatic pressure and collective diffusion, Soft Matter, 13, (2017), 9162-9173.

[25] M. Weiss, J. Maurath, N. Willenbacher, Erin Koos, Shrinkage and dimensional accuracy of porous ceramics derived from capillary suspensions, J. Euro. Ceram. Soc. 39 (2019) 1887-1892.

Acknowledgments

The authors wish to thank Mr. Mickael Faucher for the technical support regarding the cantilever method, and Dr. Benoist Naït-ALi for the scientific discussion about the drying mechanism of green ceramics.

Figure captions

Figure 1. Scheme of cantilever deflection device, with the main mechanical and geometrical properties used for the determination of in-plane stresses developed during drying. Figure 2. Mini-doctor blades with 4, 8, 12, 39 mm of blade width adapted to the spreading of slurry on the cantilever beams with 8.4, 11.7, 17.6, 44 mm of width, from the left to the right respectively.

Figure 3. Impact of ratios $\frac{E_s}{E_c(t)}$ and $\frac{h_s}{h_c}$ on the systemic error linked to the second terms of Corcoran's equation.

Figure 4. Impact of cantilever length on the deflection linked to the in-planar stress development and the mass loss linked to solvent evaporation during drying.

Figure 5. Determination of optimal length and thickness of the cantilever beam in agreement with the deflection range of the laser sensor.

Figure 6. Influence of cantilever width without the mass loss correction on the values of in-plane stress measurements, with cantilever length of 75 mm and thickness of 0.2 mm. In this study, the slurry formulation is based on the CT3000 alumina powder, as described in the section 2.2.

Figure 7. a) Influence of cantilever thickness without correction and b) with the mass loss correction on the values of in-planar stress measurements, with cantilever length of 75 mm. In this study, the slurry formulation is based on the CT3000 alumina powder, as described in the section 2.2.

Figure 8. Influence of cantilever length on the values of in-planar stress measurements during the drying with a) h_s= 0.2, b) h_s= 0.3 and c) h_s= 0.4 mm. In this study, the slurry formulation is based on the CT3000 alumina powder, as described in the section 2.2.

Figure 9. a) Evolution of shrinkage and in-plane stress during drying of a CT3000 alumina coating, with L=75 mm and hs=0.2 mm, and b) four stages of coating drying.

Figure 10. Influence of powder granulometry on the evolution of shrinkage, weight loss and in-plane stress during drying, with L=75 mm and h_s=0.2 mm. a) alumina powder with BET = 5.9 $m^2.g^{-1}$ (CT3000), b) with BET = 4.3 $m^2.g^{-1}$ (CT530), c) with BET = 2.9 $m^2.g^{-1}$ (CT1200),with BET= 2.1 $m^2.g^{-1}$ (CT530).

Table captions

Table 1: Listing of cantilever parameters reported in previous works

Table 2: Characteristics of starting alumina powders.

Table 3: Influence of coating width on the drying time, the maximum of in plane stress and the systematic error linked to mass loss during the drying.

Table 4: Characteristics of the starting alumina powders and the parameter collected from figure 10 during the drying of the alumina coatings.

Supplementary information

S1) Effective Young modulus of cantilever

In this work, the cantilever beam is slightly larger width (of 2-4mm) than the width of the coating (i.e. $b > b_s$, with b = the width of coating and b_s = the width of cantilever beam, see figure S1 on the left), to obtain a homogenous spreading of slurry on the cantilever. The Corcoran's equation describes the analytical solution of deflection linked to the in-plane stresses for a bilayer system with same width. Then, it's necessary to introduce the effective Young modulus to describe the real system by an equivalent bilayer system with the same width and corresponding equivalent mechanical behavior.

In this way, we introduce the effective Young modulus (E_s) as reported on figure S1, which is expressed as following:

$E_s = b_s/b*E$

With E: Young modulus of the steel beam, b = the width of coating and b_s = the width of cantilever beam

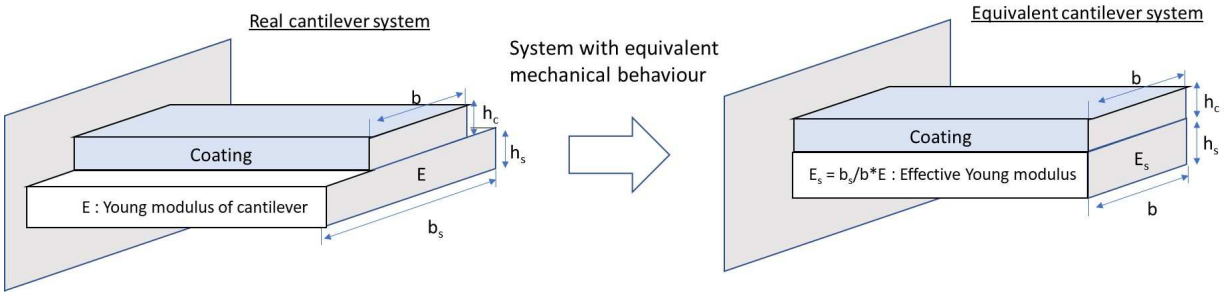

Figure S1: Effective effective young modulus of cantilever, corresponding to the analytical solution described by Corcoran's equation.

The values of effective Young modulus are reported in Table 1S in relation with the different design of cantilever used in this work.

Width of coating b (mm)	***With of cantilever b_s (mm)***	***Effective Young Modulus E_s (GPa)***
4	8.4	462
8	*11.7*	322
12	*17.6*	323
39	*44*	248

Table S1: Effective young modulus of cantilever in relation with cantilever and coating widths.

S2) Granulometry distribution of alumina powders

Figure S2 shows the particle size distribution of alumina powders obtained by laser diffraction method (Mastersizer 3000, Malvern Panalytical Ltd, UK). The powder was dispersed in a 3 mmol/l $Na_4P_2O_7$ solution and sonication (Sonopuls HD4200) was applied to deagglomerate the dispersion. It is noticeable here that CT530 alumina powder shows a bimodal distribution, with one peak close to 0.4 µm and the second other one close to 4 µm.

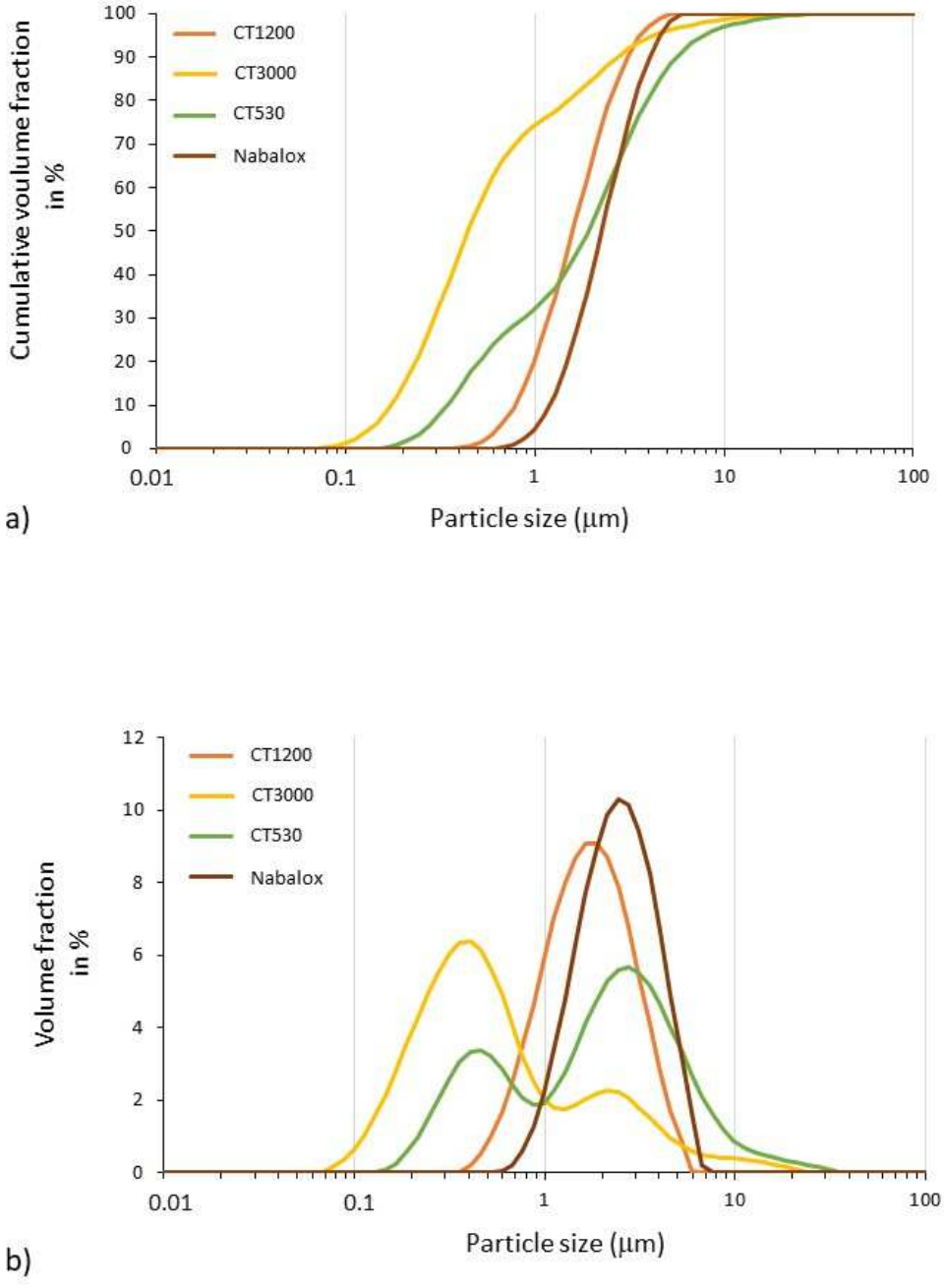

Figure S2: Particle-size distribution of alumina powders used in this work a) cumulative volume fraction and b) volume fraction in relation with particle size.

S3) Compaction front on the coating shrinkage measured by laser sensor during the drying

Figure S3 shows schematically the impact of the compaction front, due to the lateral drying, on the evolution of the coating's thickness when is measured by laser sensor. This phenomenon is well described in the literature [18-19] and it leads the migration of solvent and organics from the center to the lateral zones of the coating.

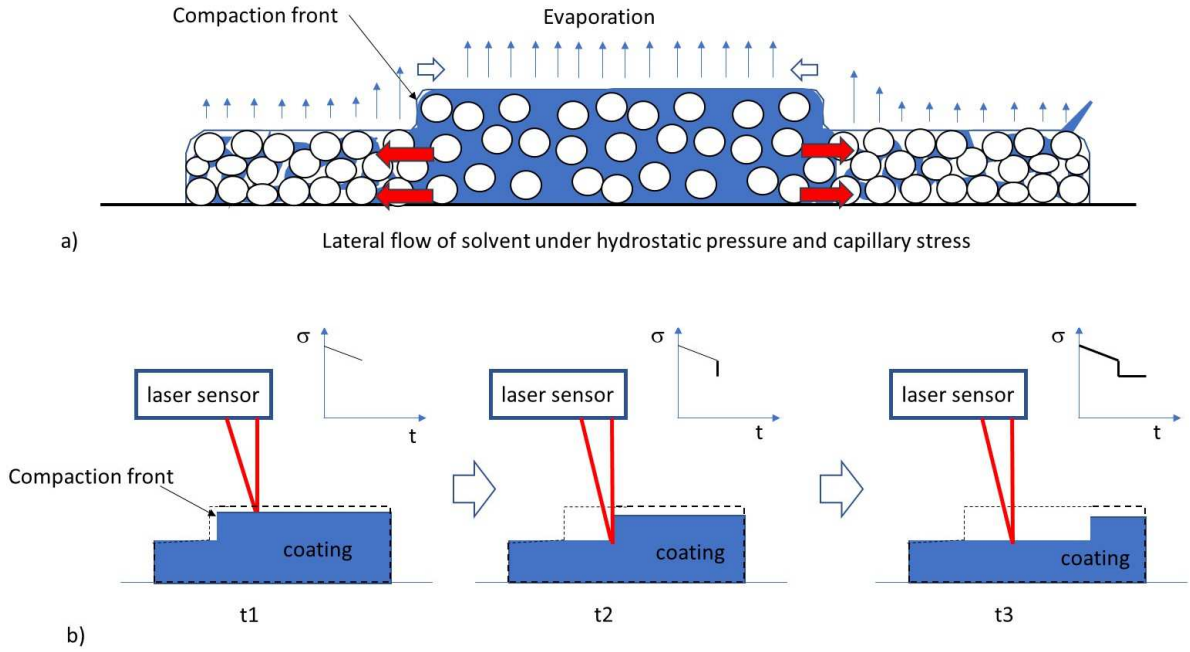

Figure S3: Impact of compaction front or lateral drying on the evolution of shrinkage measured by laser sensor during the drying.